

International Journal of Modern Physics A
 © World Scientific Publishing Company

The mass scales of the Higgs field

Maurizio Consoli

INFN - Sezione di Catania, I-95129 Catania, Italy
maurizio.consoli@ct.infn.it

Leonardo Cosmai

INFN - Sezione di Bari, I-70126 Bari, Italy
leonardo.cosmai@ba.infn.it

Received Day Month Year

Revised Day Month Year

In the first version of the theory, with a classical scalar potential, the sector inducing SSB was distinct from the Higgs field interactions induced through its gauge and Yukawa couplings. We have adopted a similar perspective but, following most recent lattice simulations, described SSB in $\lambda\Phi^4$ theory as a weak first-order phase transition. In this case, the resulting effective potential has two mass scales: i) a lower mass m_h , defined by its quadratic shape at the minima, and ii) a larger mass M_h , defined by the zero-point energy. These refer to different momentum scales in the propagator and are related by $M_h^2 \sim m_h^2 \ln(\Lambda_s/M_h)$, where Λ_s is the ultraviolet cutoff of the scalar sector. We have checked this two-scale structure with lattice simulations of the propagator and of the susceptibility in the 4D Ising limit of the theory. These indicate that, in a cutoff theory where both m_h and M_h are finite, by increasing the energy, there could be a transition from a relatively low value, e.g. $m_h=125$ GeV, to a much larger M_h . The same lattice data give a final estimate $M_h = 720 \pm 30$ GeV which induces to re-consider the experimental situation at LHC. In particular an independent analysis of the ATLAS + CMS data indicating an excess in the 4-lepton channel as if there were a new scalar resonance around 700 GeV. Finally, the presence of two vastly different mass scales, requiring an interpolating form for the Higgs field propagator also in loop corrections, could reduce the discrepancy with those precise measurements which still favor large values of the Higgs particle mass.

Keywords: Spontaneous Symmetry Breaking; Higgs field mass spectrum; LHC experiments.

PACS numbers: 11.30.Qc; 12.15.-y; 13.85.-t

1. Introduction

Spontaneous Symmetry Breaking (SSB) through the non-vanishing expectation value $\langle\Phi\rangle \neq 0$ of a self-interacting scalar field $\Phi(x)$ is the essential ingredient to generate the particle masses in the Standard Model. This old idea^{1,2} of a fundamental scalar field, in the following denoted for brevity as the Higgs field, has more recently found an important experimental confirmation after the observation, at the

Large Hadron Collider of CERN,^{3,4} of a narrow scalar resonance, of mass $m_h \sim 125$ GeV whose phenomenology fits well with the perturbative predictions of the theory. The discovery of this resonance, identified as the long sought Higgs boson, has produced the general conviction that modifications of this general picture, if any, can only come from new physics, e.g. supersymmetry.

Though, in spite of the present phenomenological consistency, this conclusion may be too premature. So far only the gauge and Yukawa couplings of the 125 GeV Higgs particle have been tested. This is the sector of the theory described by these interactions and by the associated induced coupling, say λ^{ind} , determined by

$$\frac{d\lambda^{\text{ind}}}{dt} = \frac{1}{16\pi^2} \left[-12y_t^4 + \frac{3}{4}(g')^4 + \frac{3}{2}(g')^2 g^2 + \frac{9}{4}g^4 \right] \quad (1)$$

where g and g' are the SU(2) \times U(1) gauge couplings and we have just restricted to the quark-top Yukawa coupling y_t evolving according to

$$\frac{dy_t}{dt} = \frac{1}{16\pi^2} \left[\frac{9}{2}y_t^3 - \left(\frac{17}{12}(g')^2 + \frac{9}{4}g^2 + 8g_3^2 \right) y_t \right] \quad (2)$$

where g_3 is the SU(3)_c coupling. Instead, the effects of a genuine scalar self-coupling λ , if any, are below the accuracy of the measurements. For this reason, an uncertainty about the mechanisms at the base of symmetry breaking still persists.

We briefly mention that, at the beginning, SSB was explained in terms of a classical scalar potential with a double-well shape. Only later, after the work of Coleman and Weinberg,⁵ it became increasingly clear that the phenomenon should be described at the quantum level and that the classical potential had to be replaced by the effective potential $V_{\text{eff}}(\varphi)$ which includes the zero-point energy of all particles in the spectrum. This has produced the present view where the description of SSB is demanded to the combined study of all couplings and of their evolution up to very large energy scales.

But, in principle, SSB could still be determined by the pure scalar sector if the contribution of the other fields to the vacuum energy is negligible. This may happen if, as in the original picture with the classical potential, the primary mechanism producing SSB is quite distinct from the remaining Higgs field self-interactions induced through the gauge and Yukawa couplings. The type of scenario we have in mind is sketched below:

i) One could first take into account the indications of most recent lattice simulations of pure $\lambda\Phi^4$ in 4D.^{6–8} These calculations, performed in the Ising limit of the theory with different algorithms, indicate that on the largest lattices available so far the SSB phase transition is (weakly) first order.

ii) With a first-order transition, SSB would emerge as a true instability of the symmetric vacuum at $\varphi = 0$. Its quanta have a tiny and still positive mass squared $V''_{\text{eff}}(\varphi = 0) = m_\Phi^2 > 0$ but, nevertheless, their interactions can destabilize this symmetric vacuum⁹ and produce the condensation process responsible for symmetry breaking. This primary $\lambda\Phi^4$ sector should be considered with its own degree of

locality defined by some cutoff scale Λ_s . We are thus lead to identify Λ_s as the Landau pole for a bare coupling $\lambda_B = +\infty$. This corresponds precisely to the Ising limit and provides the best possible definition of a local $\lambda\Phi^4$ for any non-zero low-energy coupling $\lambda \sim 1/\ln \Lambda_s \ll 1$. This is the relevant one for low-energy physics, as in the original Coleman-Weinberg calculation of the effective potential at $\varphi^2 \ll \Lambda_s^2$.

iii) After this first step, the description of the basic $\lambda\Phi^4$ sector can further be improved by going to a next level. Since, for any non-zero λ , there is a finite Landau pole, one can consider the whole set of theories (Λ_s, λ) , (Λ'_s, λ') , (Λ''_s, λ'') ...with larger and larger Landau poles, smaller and smaller low-energy couplings but all having the same depth of the potential, i.e. with the same vacuum energy $\mathcal{E} = V_{\text{eff}}(\langle\Phi\rangle)$. This requirement derives from imposing the RG-invariance of the effective potential in the three-dimensional space $(\varphi, \lambda, \Lambda_s)$ and, in principle, allows one to handle the $\Lambda_s \rightarrow \infty$ limit ^a. In this formalism, besides a first invariant mass scale \mathcal{I}_1 , defined by $|\mathcal{E}| \sim \mathcal{I}_1^4$, there is a second invariant \mathcal{I}_2 , related to a particular normalization of the vacuum field, which is the natural candidate to represent the weak scale $\mathcal{I}_2 = \langle\Phi\rangle \sim 246$ GeV. The minimization of the effective potential can then be expressed as a relation $\mathcal{I}_1 = K\mathcal{I}_2$ in terms of some proportionality constant K .

This RG-analysis of the effective potential, discussed in Sects.2 and 3, is the main point of this paper. It takes into account that, in those approximation schemes that reproduce the type of weak first-order phase transition favored by recent lattice simulations, there are *two* vastly different mass scales, say m_h and M_h . These are defined respectively by the second derivative and the depth of the effective potential at its minima and related by $M_h^2 \sim L m_h^2 \gg m_h^2$ where $L = \ln(\Lambda_s/M_h)$. Therefore, even though $(m_h/\langle\Phi\rangle)^2 \sim 1/L$, the larger $M_h = \mathcal{I}_1$ remains finite in units of $\mathcal{I}_2 = \langle\Phi\rangle$.

To appreciate the change of perspective, let us recall the usual description of a second-order phase transition as summarized in the scalar potential reported in the Review of Particle Properties.¹⁰ In this review, which gives the present interpretation of the theory in the light of most recent experimental results, the scalar potential is expressed as (PDG=Particle Data Group)

$$V_{\text{PDG}}(\varphi) = -\frac{1}{2}m_{\text{PDG}}^2\varphi^2 + \frac{1}{4}\lambda_{\text{PDG}}\varphi^4 \quad (3)$$

By fixing $m_{\text{PDG}} \sim 88.8$ GeV and $\lambda_{\text{PDG}} \sim 0.13$, this potential has a minimum at $|\varphi| = \langle\Phi\rangle \sim 246$ GeV and quadratic shape $V''_{\text{PDG}}(\langle\Phi\rangle) = (125 \text{ GeV})^2$. Note that, as a built-in relation, the second derivative of the potential $(125 \text{ GeV})^2$ also determines its depth, i.e. the vacuum energy \mathcal{E}_{PDG}

$$\mathcal{E}_{\text{PDG}} = -\frac{1}{2}m_{\text{PDG}}^2\langle\Phi\rangle^2 + \frac{1}{4}\lambda_{\text{PDG}}\langle\Phi\rangle^4 = -\frac{1}{8}(125 \text{ GeV}\langle\Phi\rangle)^2 \sim -1.2 \cdot 10^8 \text{ GeV}^4 \quad (4)$$

^aThis limit should also be considered because the scalar sector is assumed to induce SSB and thus to determine the vacuum structure and its symmetries. In a quantum field theory, imposing invariance under RG-transformations is then the standard method to remove the ultraviolet cutoff or, in alternative, to minimize its influence on observable quantities.

Instead in our case, by identifying $m_h \sim 125$ GeV, the vacuum energy $\mathcal{E} \sim -\frac{1}{8}M_h^2\langle\Phi\rangle^2$ would be deeper than Eq.(4) by the potentially divergent factor L . Thus, it would also be insensitive to the other sectors of the theory, e.g. the gauge and Yukawa interactions, whose effect is just to replace the scalar self coupling λ with the total coupling $\lambda^{\text{tot}} = \lambda + \lambda^{\text{ind}}$ in the definition of the quadratic shape of the effective potential. All together, once the picture sketched above works also in the $\Lambda_s \rightarrow \infty$ limit, where λ becomes extremely small at any finite energy scale, the phenomenology of the 125 GeV resonance would remain the same and SSB would essentially be determined by the pure scalar sector.

We emphasize that the relation $M_h = K\langle\Phi\rangle$ is not introducing a new large coupling $K^2 = O(1)$ in the picture of symmetry breaking. This K^2 should not be viewed as a coupling constant or, at least, as a coupling constant which produces *observable* interactions in the broken symmetry phase. From this point of view, it may be useful to compare SSB to the phenomenon of superconductivity in non-relativistic solid state physics. There the transition to the new, superconductive phase represents an essential instability that occurs for any infinitesimal two-body attraction ϵ between the two electrons forming a Cooper pair. At the same time, however, the energy density of the superconductive phase and all global quantities of the system (energy gap, critical temperature, etc.) depend on the much larger collective coupling ϵN obtained after re-scaling the tiny 2-body strength by the large number of states near the Fermi surface. This means that, in principle, the same macroscopic description could be obtained with smaller and smaller ϵ and Fermi systems of corresponding larger and larger N . In this comparison λ is the analog of ϵ and K^2 is the analog of ϵN .

Another aspect, implicit in the usual picture of SSB, is that $V''_{\text{PDG}}(\langle\Phi\rangle)$, which strictly speaking is the self-energy function at zero momentum $|\Pi(p=0)|$, is assumed to coincide with the pole of the Higgs propagator. As discussed in Sect.4, m_h and M_h refer to different momentum regions in the connected scalar propagator $G(p) = 1/(p^2 - \Pi(p))$, namely m_h for $p \rightarrow 0$ and M_h at larger p . Therefore, if Λ_s were large but finite, so that both m_h and M_h are finite, the transition between the two scales should become visible by increasing the energy.

In Sect.5, we will show that this two-scale structure is supported by lattice simulations in the 4D Ising limit of the theory. In fact, once m_h^2 is directly computed from the zero-momentum connected propagator $G(p=0)$ (the inverse susceptibility) and M_h is extracted from the behaviour of $G(p)$ at higher momentum, the lattice data confirm the increasing expected logarithmic trend $M_h^2 \sim Lm_h^2$.

From a phenomenological point of view, these simulations indicate that a relatively low value, e.g. $m_h=125$ GeV, could in principle coexist with a much larger M_h . By combining various lattice determinations, our final estimate $M_h = 720 \pm 30$ GeV will lead us to re-consider, in Sect.6, the experimental situation at LHC. In particular, an independent analysis¹¹ of the ATLAS + CMS data indicating an excess in the 4-lepton channel as if there were a new scalar resonance around 700 GeV. This excess, if confirmed, could indicate the second heavier mass scale discussed in

this paper. Then, differently from the low-mass state at 125 GeV, the decay width of such heavy state into longitudinal vector bosons will be crucial to determine the strength of the *observable* scalar self-coupling and the degree of locality of the theory.

Finally, the simultaneous presence of two mass scales would also require an interpolating parametrization for the Higgs field propagator in loop corrections. This could help to reduce the 3-sigma discrepancies with those precision measurements which still favor rather large values of the Higgs particle mass.

2. The one-loop effective potential

To study SSB in $\lambda\Phi^4$ theory, the crucial quantity is the physical, mass squared parameter $m_\Phi^2 = V''_{\text{eff}}(\varphi = 0)$ introduced by first quantizing the theory in the symmetric phase at $\varphi = 0$. A first-order scenario corresponds to a phase transition occurring at some small but still positive m_Φ^2 . In this case, the symmetric vacuum, although *locally* stable (because its excitations have a physical mass $m_\Phi^2 > 0$), would be *globally* unstable in some range of mass below a critical value, say $0 \leq m_\Phi^2 < m_c^2$. If m_c^2 is extremely small, however, one speaks of a *weak* first-order transition to mean that it would become indistinguishable from a second-order transition if one does not look on a fine enough scale.

This first-order scenario is equivalent to say that the lowest energy state of the massless theory at $m_\Phi^2 = 0$ corresponds to the broken-symmetry phase, as suggested by Coleman and Weinberg⁵ in their one-loop calculation. This represents the simplest scheme which is consistent with this picture. We will first reproduce below this well known computation and exploit its implications. A discussion on the general validity of the one-loop approximation is postponed to the following section.

The Coleman-Weinberg potential is

$$V_{\text{eff}}(\varphi) = \frac{\lambda}{4!}\varphi^4 + \frac{\lambda^2}{256\pi^2}\varphi^4 \left[\ln(\tfrac{1}{2}\lambda\varphi^2/\Lambda_s^2) - \frac{1}{2} \right] \quad (5)$$

and its first few derivatives are

$$V'_{\text{eff}}(\varphi) = \frac{\lambda}{6}\varphi^3 + \frac{\lambda^2}{64\pi^2}\varphi^3 \ln(\tfrac{1}{2}\lambda\varphi^2/\Lambda_s^2) \quad (6)$$

and

$$V''_{\text{eff}}(\varphi) = \frac{\lambda}{2}\varphi^2 + \frac{3\lambda^2}{64\pi^2}\varphi^2 \ln(\tfrac{1}{2}\lambda\varphi^2/\Lambda_s^2) + \frac{\lambda^2\varphi^2}{32\pi^2} \quad (7)$$

We observe that, by introducing the mass squared parameter

$$M^2(\varphi) \equiv \tfrac{1}{2}\lambda\varphi^2 \quad (8)$$

the one-loop potential can be expressed as a classical background + zero-point energy of a particle with mass $M(\varphi)$ (after subtraction of constant terms and of

6 *M. Consoli, L. Cosmai*

quadratic divergences), i.e.

$$V_{\text{eff}}(\varphi) = \frac{\lambda\varphi^4}{4!} - \frac{M^4(\varphi)}{64\pi^2} \ln \frac{\Lambda_s^2 \sqrt{e}}{M^2(\varphi)} \quad (9)$$

Thus, non-trivial minima of $V_{\text{eff}}(\varphi)$ occur at those points $\varphi = \pm v$ where ^b

$$M_h^2 \equiv M^2(\pm v) = \frac{\lambda v^2}{2} = \Lambda_s^2 \exp\left(-\frac{32\pi^2}{3\lambda}\right) \quad (10)$$

so that

$$m_h^2 \equiv V_{\text{eff}}''(\pm v) = \frac{\lambda^2 v^2}{32\pi^2} = \frac{\lambda}{16\pi^2} M_h^2 \sim \frac{M_h^2}{L} \ll M_h^2 \quad (11)$$

where $L \equiv \ln \frac{\Lambda_s}{M_h}$. Notice that the energy density depends on M_h and *not* on m_h , because

$$\mathcal{E} = V_{\text{eff}}(\pm v) = -\frac{M_h^4}{128\pi^2} \quad (12)$$

therefore the critical temperature at which symmetry is restored, $k_B T_c \sim M_h$, and the stability conditions of the broken phase depends on the larger M_h and not on the smaller scale m_h .

These are the results for the $m_\Phi = 0$ case. To study the phase transition for a small $m_\Phi^2 > 0$, we will just quote the results of Ref.⁹ In this case, the one-loop potential has the form

$$V_{\text{eff}}(\varphi) = \frac{1}{2} m_\Phi^2 \varphi^2 + \frac{\lambda\varphi^4}{4!} + \frac{M^4(\varphi)}{64\pi^2} \left[\ln \frac{M^2(\varphi)}{\sqrt{e}\Lambda_s^2} + F\left(\frac{m_\Phi^2}{M^2(\varphi)}\right) \right] \quad (13)$$

where

$$F(y) = \ln(1+y) + \frac{y(4+3y)}{2(1+y)^2} \quad (14)$$

Then, by introducing the mass-squared parameter Eq.(10) of the $m_\Phi = 0$ case, the condition for non-trivial minima $\varphi = \pm v$ for $m_\Phi \neq 0$, can be expressed as⁹

$$m_\Phi^2 \leq \frac{\lambda M_h^2}{64\pi^2 \sqrt{e}} \equiv m_c^2 \quad (15)$$

Since the critical mass for the phase transition vanishes, in units of M_h , in the $\Lambda_s \rightarrow \infty$ limit

$$\frac{m_c^2}{M_h^2} \sim \frac{1}{L} \rightarrow 0 \quad (16)$$

SSB emerges as an infinitesimally weak first-order transition.

Notice that this critical mass has the same typical magnitude as the quadratic shape m_h^2 in Eq.(11). In this sense, by requiring SSB, we are establishing a mass

^bIn view of a possible ambiguity in the normalization of the vacuum field, that may affect the identification of the weak scale $\langle \Phi \rangle \sim 246$ GeV, we will for the moment denote as $\varphi = \pm v$ the minima entering the computation of the effective potential.

hierarchy.⁹ On the one hand, the tiny mass of the symmetric phase $m_\Phi^2 \leq m_c^2$ and the similar infinitesimal quadratic shape m_h^2 of the potential at its minima. On the other hand, the much larger M_h^2 entering the zero-point energy which destabilizes the symmetric phase^c.

As anticipated in the Introduction, to improve our analysis of the primary $\lambda\Phi^4$ sector, we will now consider the whole set of pairs $(\Lambda_s, \lambda), (\Lambda'_s, \lambda'), (\Lambda''_s, \lambda'')$...with different Landau poles and corresponding low-energy couplings. The correspondence is such to obtain the same value for the vacuum energy Eq.(12), or equivalently for the mass scale Eq.(10), and thus the cutoff independence of the result by requiring

$$\left(\Lambda_s \frac{\partial}{\partial \Lambda_s} + \Lambda_s \frac{\partial \lambda}{\partial \Lambda_s} \frac{\partial}{\partial \lambda} \right) \mathcal{E}(\lambda, \Lambda_s) = 0 \quad (17)$$

By assuming Eq.(12) and with the definition

$$\Lambda_s \frac{\partial \lambda}{\partial \Lambda_s} \equiv -\beta(\lambda) = -\frac{3\lambda^2}{16\pi^2} + O(\lambda^3) \quad (18)$$

the solution is thus $|\mathcal{E}| \sim \mathcal{I}_1^4$, where \mathcal{I}_1 is the first RG-invariant^d

$$\mathcal{I}_1 = M_h = \Lambda_s \exp\left(\int^\lambda \frac{dx}{\beta(x)}\right) \sim \Lambda_s \exp\left(-\frac{16\pi^2}{3\lambda}\right) \quad (19)$$

The above relations derive from the more general requirement of RG-invariance of the effective potential in the three-dimensional space $(\varphi, \lambda, \Lambda_s)$

$$\left(\Lambda_s \frac{\partial}{\partial \Lambda_s} + \Lambda_s \frac{\partial \lambda}{\partial \Lambda_s} \frac{\partial}{\partial \lambda} + \Lambda_s \frac{\partial \varphi}{\partial \Lambda_s} \frac{\partial}{\partial \varphi} \right) V_{\text{eff}}(\varphi, \lambda, \Lambda_s) = 0 \quad (20)$$

In fact, at the minima $\varphi = \pm v$, where $(\partial V_{\text{eff}}/\partial \varphi) = 0$, Eq.(17) is a direct consequence of Eq.(20).

Another consequence of this RG-analysis is that, by introducing an anomalous dimension for the vacuum field

$$\Lambda_s \frac{\partial \varphi}{\partial \Lambda_s} \equiv \gamma(\lambda)\varphi \quad (21)$$

^cThe analysis for the one-component scalar field can be easily extended to a continuous symmetry $O(N)$ theory. To this end, it is convenient to follow ref.¹² where it is shown that the one-loop potential is only due to the zero-point energy associated with the radial field $\rho(x)$, the contribution from the Goldstone bosons being exactly canceled by the change in the quantum measure $(\text{Det}\rho)$.

^d Note the minus sign in the definition of the β -function. This is because we are differentiating the coupling constant $\lambda = \lambda(\mu, \Lambda_s)$, at a certain scale $\mu = M_h$ and with cutoff Λ_s , with respect to the cutoff and not with respect to μ . Namely, at fixed μ , we are considering different integral curves so that λ has to decrease by increasing Λ_s . Also, to use consistently the 1-loop β -function in Eq.(19), the integral at the exponent should be considered a definite integral that only depends on λ because its other limit, say $\lambda_0 > \lambda$, is kept fixed and such that, for $x < \lambda_0$, one can safely neglect $O(x^3)$ terms in $\beta(x)$. Therefore, since λ_0 cannot be too large, there is a relative λ -independent factor $\exp(\frac{16\pi^2}{3\lambda_0}) \gg 1$ between Eq.(10) and Eq.(19). Strictly speaking, this means that, to obtain the same physical M_h from Eq.(10) and Eq.(19), one should use vastly different values of Λ_s . This is a typical example of cutoff artifact.

8 *M. Consoli, L. Cosmai*

there is a second invariant associated with the RG-flow in the $(\varphi, \lambda, \Lambda_s)$ space, namely

$$\mathcal{I}_2(\varphi) = \varphi \exp\left(\int^\lambda dx \frac{\gamma(x)}{\beta(x)}\right) \quad (22)$$

which introduces a particular normalization of φ . This had to be expected because from Eq.(10) the cutoff-independent combination is

$$\lambda v^2 \sim M_h^2 = \mathcal{I}_1^2 \quad (23)$$

and not v^2 itself, thus implying $\gamma = \beta/(2\lambda)$ ^e. Therefore, the condition for the minimum of the effective potential can be expressed as a proportionality relation between the two invariants in terms of some constant K , say

$$\mathcal{I}_1 = K \mathcal{I}_2(v) \quad (24)$$

Then, with the aim of extending our description of SSB to the Standard Model, a question naturally arises. Suppose that, as in the first version of the theory, SSB is essentially generated in the pure scalar sector and the other couplings are just small perturbative corrections. When we couple scalar and gauge fields, and we want to separate the field in a vacuum component and a fluctuation, which is the correct definition of the weak scale $\langle \Phi \rangle \sim 246$ GeV? A first possibility would be to identify $\langle \Phi \rangle$ with the same v considered so far which in general, i.e. beyond the Coleman-Weinberg limit, is related to M_h through a relation similar to Eq.(10), say

$$v^2 \sim L M_h^2 = L \mathcal{I}_1^2 \quad (25)$$

But $\langle \Phi \rangle \sim 246$ GeV is a basic entry of the theory (as the electron mass and fine structure constant in QED). For such a fundamental quantity, once we are trying to describe SSB in a cutoff-independent way, it would be more appropriate a relation with the second invariant, i.e.

$$\langle \Phi \rangle^2 = \mathcal{I}_2^2(v) = \frac{\mathcal{I}_1^2}{K^2} = \frac{M_h^2}{K^2} \quad (26)$$

so that both $\langle \Phi \rangle^2 \sim (v^2/L)$ and $M_h^2 \sim (v^2/L)$ are cutoff-independent quantities. If we adopt this latter choice, the proportionality can then be fixed through the generalization of Eq.(11) in terms of some constant c_2

$$V_{\text{eff}}''(\pm v) = m_h^2 \sim \frac{c_2 M_h^2}{L} \quad (27)$$

^eWe emphasize that this is the anomalous dimension of the *vacuum* field φ which is the argument of the effective potential. As such, it is quite unrelated to the more conventional anomalous dimension of the *shifted* field as obtained from the residue of the connected propagator $Z = Z_{\text{prop}} = 1 + O(\lambda)$. By “triviality”, the latter is constrained to approach unity in the continuum limit. To better understand the difference, it is useful to regard symmetry breaking as a true condensation phenomenon⁹ associated with the macroscopic occupation the same quantum state $\mathbf{k} = 0$. Then φ is related to the condensate while the shifted field is related to the modes at $\mathbf{k} \neq 0$ which are not macroscopically populated. Numerical evidence for these two different re-scalings will be provided in Sect.5. In fact, the logarithmic increasing L relating v^2 and $\langle \Phi \rangle^2$ is the counterpart^{13,14} of the logarithmic increasing L between M_h^2 and m_h^2 which can be observed on the lattice.

and the traditional definition of $\langle\Phi\rangle$ from the quadratic shape of the effective potential

$$V''_{\text{eff}}(\pm v) = m_h^2 = \frac{\lambda\langle\Phi\rangle^2}{3} \sim \frac{16\pi^2}{9L}\langle\Phi\rangle^2 \quad (28)$$

This gives

$$M_h \sim \frac{4\pi}{3\sqrt{c_2}}\langle\Phi\rangle \equiv K\langle\Phi\rangle \quad (29)$$

in terms of the constant c_2 that, in Sect.5, will be estimated from lattice simulations of the theory.

3. On the validity of the one-loop potential

Following the lattice simulations of refs.,^{6–8} which support the picture of SSB in $\lambda\Phi^4$ as a weak first-order transition, we have considered in Sect.2 the simplest approximation scheme which is consistent with this scenario, namely the one-loop effective potential. From its functional form and its minimization conditions, we have also argued that this simplest scheme can become the basis for an alternative approach to the ideal continuum limit such that the vacuum energy \mathcal{E} and the natural definition of the Standard Model weak scale $\langle\Phi\rangle \sim 246$ GeV are both finite, cutoff independent quantities.

But one may object that, as remarked by Coleman and Weinberg already in 1973, the straightforward minimization procedure followed in our Sect.2, and used to derive \mathcal{E} and $\langle\Phi\rangle$, can be questioned. The point is that by performing the standard Renormalization Group (RG) “improvement” of the one-loop potential, all leading-logarithmic terms are reabsorbed into a positive running coupling constant $\lambda(\varphi)$. Thus, by preserving the positivity of $\lambda(\varphi)$, the one-loop minimum disappears and one would now predict a second-order transition at $m_\Phi^2 = 0$, as in the classical potential. The conventional view is that the latter result is trustworthy while the former is not. The argument is that the one-loop potential’s non-trivial minimum occurs where the one-loop “correction” term is as large as the tree-level term. However, also this standard RG-improved result can be questioned because, near the one-loop minimum, the convergence of the resulting geometric series of leading logs is not so obvious.

To gain insight, one can then compare with other approximation schemes, for instance the Gaussian approximation^{15,16} which has a variational nature and explores the Hamiltonian in the class of the Gaussian functional states. It also represents a very natural alternative because, at least in the continuum limit, a Gaussian structure of Green’s functions fits with the generally accepted “triviality” of the theory in 3+1 dimensions. This other calculation produces a result in agreement with the one-loop potential.^{13,14} This agreement does not mean that there are no non-vanishing corrections beyond the one-loop level; there are, but those additional terms do not alter the functional form of the result. The point is that, again, as in

10 *M. Consoli, L. Cosmai*

$$\begin{aligned}
 \text{"}\lambda\Phi^4\text{"} &= \text{diagram 1} + \text{diagram 2} + \text{higher orders} \\
 &\quad \downarrow \\
 \text{"}\lambda\Phi^4\text{"} &= \left[\text{diagram 1} + \text{diagram 2 (uv-finite)} \right] + \text{diagram 3 (uv-divergent)} + \text{higher orders}
 \end{aligned}$$

Fig. 1. The re-arrangement of the perturbative expansion considered by Stevenson²¹ in his alternative RG-analysis of the effective potential. Besides the tree-level $+\lambda\delta^3(\mathbf{r})$ repulsion, the quanta of the symmetric phase, with mass m_Φ , feel a $-\lambda^2 \frac{e^{-2m_\Phi r}}{r^3}$ attraction from the Fourier transform of the second diagram in square bracket⁹ whose range becomes longer and longer in the $m_\Phi \rightarrow 0$ limit. For m_Φ below a critical mass m_c , this dominates and induces SSB in the one-loop potential. Since the higher-order terms just renormalize these two basic effects, the RG-improved effective potential, in this new scheme, confirms the same scenario of the one loop approximation.

the one-loop approximation, the gaussian effective potential can be expressed as a classical background + zero-point energy with a φ -dependent mass as in Eq.(9)^f, i.e.

$$V_{\text{eff}}^G(\varphi) = \frac{\hat{\lambda}\varphi^4}{4!} - \frac{\Omega^4(\varphi)}{64\pi^2} \ln \frac{\Lambda_s^2 \sqrt{e}}{\Omega^2(\varphi)} \quad (30)$$

with

$$\hat{\lambda} = \frac{\lambda}{1 + \frac{\lambda}{16\pi^2} \ln \frac{\Lambda_s}{\Omega(\varphi)}} \quad (31)$$

and

$$\Omega^2(\varphi) = \frac{\hat{\lambda}\varphi^2}{2} \quad (32)$$

This explains why the one-loop potential can also admit a non-perturbative interpretation. It is the prototype of the gaussian and post-gaussian calculations^{19,20} where higher-order contributions to the energy density are effectively reabsorbed into the same basic structure: a classical background + zero-point energy with a φ -dependent mass. But, even by taking into account the indications of lattice simulations,⁶⁻⁸ and having at hand the explicit one-loop and gaussian calculations Eqs.(9) and (30), a skeptical reader may still be reluctant to abandon the standard second-order scenario. He would like a general argument explaining why the

^fAs already remarked for the one-loop potential, also for the Gaussian effective potential the zero-point energy in a spontaneously broken $O(N)$ theory is just due to the shifted radial field. For the Gaussian approximation this requires the diagonalization^{17,18} of the mass matrix to explicitly display a spectrum with one massive field and $(N-1)$ massless fields as required by the Goldstone theorem.

standard RG-analysis, which predicts the correct Λ_s -dependence of the low-energy coupling, fails instead to predict the order of the phase transition.

Finding such a general argument was, indeed, the motivation of ref.⁹ : understanding the physical mechanisms at the base of SSB as a first-order transition. Here, the crucial observation was that the quanta of the symmetric phase, the “phions”,⁹ besides the $+\lambda\delta^3(\mathbf{r})$ tree-level repulsion, also feel a $-\lambda^2 \frac{e^{-2m_\Phi r}}{r^3}$ attraction which shows up at the one-loop level and whose range becomes longer and longer in the $m_\Phi \rightarrow 0$ limit ^g. By taking into account both effects, a calculation of the energy density in the dilute-gas approximation,⁹ which is equivalent to the one-loop potential, indicates that for small m_Φ the lowest-energy state is not the empty state with no phions but a state with a non-zero density of phions Bose condensed in the zero-momentum mode. The instability corresponds to spontaneous symmetry breaking and happens when the phion’s physical mass m_Φ^2 is still positive.

Then, if one thinks that SSB originates from these two qualitatively different competing effects, one can now understand why the standard RG-resummation fails to predict the order of the phase transition. In fact, the one-loop attractive term originates from the *ultraviolet finite* part of the one-loop diagrams. Therefore, the correct way to include higher order terms in the effective potential is to renormalize *both* the tree-level repulsion and the long-range attraction, as in a theory with *two* coupling constants ^h. This strategy, which is clearly different from the usual one, has been implemented by Stevenson,²¹ see Fig.1. In this new scheme, one can obtain SSB without violating the positivity of $\lambda(\varphi)$ so that one-loop effective potential and its RG-group improvement now agree very well. Stevenson’s analysis confirms the weak first-order scenario and the same two-mass picture $M_h^2 \sim m_h^2 \ln(\Lambda_s/M_h)$.

4. m_h and M_h : the quasi-particles of the broken phase

After having described the various aspects and the general validity of the one-loop calculation, let us now try to sharpen the meaning of the two mass scales m_h and M_h . To this end, we will first express the inverse propagator in its general form in terms of the 2-point self-energy function $\Pi(p)$

$$G^{-1}(p) = p^2 - \Pi(p) \quad (33)$$

Then, since the derivatives of the effective potential produce (minus) the n-point functions at zero external moment, our smaller mass can be expressed as

$$m_h^2 \equiv V''_{\text{eff}}(\varphi = \pm v) = -\Pi(p=0) = |\Pi(p=0)| \quad (34)$$

so that $G^{-1}(p) \sim p^2 + m_h^2$ for $p \rightarrow 0$.

^gStarting from the scattering matrix element \mathcal{M} , obtained from Feynman diagrams, one can construct an interparticle potential that is basically the 3-dimensional Fourier transform of \mathcal{M} , see the articles of Feinberg et al.^{22,23}

^hThis is similar to what happens in scalar electrodynamics.⁵ There, if the scalar self-coupling is not too large, no conflict arises between one-loop potential and its standard RG-improvement.

As far as M_h is concerned, we can instead use the relation of the zero-point-energy (“zpe”) in Eq.(9) to the trace of the logarithm of the inverse propagator

$$zpe = \frac{1}{2} \int \frac{d^4 p}{(2\pi)^4} \ln(p^2 - \Pi(p)) \quad (35)$$

Then, after subtraction of constant terms and of quadratic divergences, to match the one-loop form in Eq.(9), we can impose suitable lower and upper limits to the p -integration in the logarithmic divergent part (i.e. $p_{\max}^2 \sim \sqrt{e}\Lambda_s^2$ and $p_{\min}^2 \sim M_h^2$)

$$zpe = -\frac{1}{4} \int_{p_{\min}}^{p_{\max}} \frac{d^4 p}{(2\pi)^4} \frac{\Pi^2(p)}{p^4} \sim -\frac{\langle \Pi^2(p) \rangle}{64\pi^2} \ln \frac{p_{\max}^2}{p_{\min}^2} \sim -\frac{M_h^4}{64\pi^2} \ln \frac{\sqrt{e}\Lambda_s^2}{M_h^2} \quad (36)$$

This shows that the quartic term M_h^4 is associated with the typical, average value $\langle \Pi^2(p) \rangle$ at non-zero momentum. Thus, if we trust in the one-loop relation $M_h^2 \sim m_h^2 \ln \frac{\Lambda_s}{M_h}$, there should be substantial deviations when trying to extrapolate the propagator to the higher-momentum region with the same 1-particle form $G^{-1}(p) \sim p^2 + m_h^2$ which controls the $p \rightarrow 0$ limit.

Before considering deviations of the propagator from the standard 1-particle form, one should first envisage what kind of constraints are placed by “triviality”. This dictates a continuum limit as a generalized free-field theory, i.e. where all interaction effects are reabsorbed into the first two moments of a Gaussian distributions. Therefore, in this limit, the spectrum can just contain free massive particles.

However Stevenson’s alternative RG-analysis,²¹ besides confirming the two-scale structure $M_h^2 \sim m_h^2 \ln(\Lambda_s/M_h)$ found at one loop, also indicates how to recover the massive free-field limit in an unconventional way. In fact, his propagator interpolates between $G^{-1}(p=0) = m_h^2$ and $G^{-1}(p) \sim (p^2 + M_h^2)$ at momenta $p^2 \gg m_h^2$, see his Eqs.(16)–(22). This suggests the general following form of the propagator

$$G^{-1}(p) = (p^2 + M_h^2)f(p) \quad (37)$$

with $f(p) \sim (m_h/M_h)^2$ in the $p \rightarrow 0$ limit and $f(p) \rightarrow 1$ for momenta $p^2 \gg m_h^2$. Also, note that his Eq.(23) should be read as $G^{-1}(p)$ and that he considers the continuum limit $(m_h/M_h)^2 \rightarrow 0$. Then $f(p)$ becomes a step function which is unity for any finite p (i.e. for any p finite in units of M_h) except for a discontinuity at $p = 0$ where $f = 0$. Up to this discontinuity in the zero-measure set $p = 0$, one then re-discovers the usual trivial continuum limit with just one massive free particle¹.

We are thus lead to consider the following picture of the cutoff theory where both m_h and M_h are finite, albeit vastly different scales. This picture introduces two types of “quasi-particles”: quasi-particles of type I, with mass m_h , and quasi-particles of type II, with mass M_h . The quasi-particles of type I are the weakly coupled excitations of the broken-symmetry phase in the low-momentum region. By increasing the momentum these first quasi-particle states become more strongly

¹Note that $p = 0$ represents a Lorentz-invariant set being transformed into itself under any transformation of the Poincaré Group. Thus, in principle, a continuum limit with a discontinuity in the zero-measure set $p = 0$ is not forbidden in translational invariant vacua as with SSB.

coupled. However, the constraint placed by “triviality” is that, by approaching the continuum limit, all interaction effects have to be effectively reabsorbed into the mass of other quasi-particles, those of type II, i.e. into the parameter we have called M_h . The very large difference between M_h and m_h , expected from our analysis of the effective potential, implies that at higher momentum the self-coupling of quasi-particles of type I becomes substantial but, nevertheless, will remain hidden in the transition from m_h to M_h . In an ideal continuum limit, the whole low-momentum region for the quasi-particles of type I reduces to the zero-measure set $p = 0$ and one is just left^j with the quasi-particles of type II with mass M_h .

To show that this new interpretation of “triviality” is not just speculation, in the following section, we will report the results of lattice simulations of the broken-symmetry phase which support our two-mass picture.

5. Comparison with lattice simulations

We will now compare the two-mass picture of Sects.2-4 with the results of lattice simulations in the broken-symmetry phase of $\lambda\Phi^4$ in 4D. These simulations have been performed in the Ising limit of the theory governed by the lattice action

$$S_{\text{Ising}} = -\kappa \sum_x \sum_{\mu} [\phi(x + \hat{e}_{\mu})\phi(x) + \phi(x - \hat{e}_{\mu})\phi(x)] \quad (38)$$

with the lattice field $\phi(x)$ taking only the values ± 1 . Also, the broken-symmetry phase corresponds to $\kappa > \kappa_c$, this critical value being now precisely determined as $\kappa_c = 0.0748474(3)$.^{6,7}

Addressing to^{24,25} for the various aspects of the analysis, we recall that the Ising limit is traditionally considered a convenient laboratory for a non-perturbative study of the theory. As anticipated in the Introduction, it corresponds to a $\lambda\Phi^4$ with an infinite bare coupling, as if one were sitting precisely at the Landau pole. In this sense, for any finite cutoff, it provides the best definition of the local limit for a given value of the renormalized parameters.

Using the Swendsen-Wang²⁶ and Wolff²⁷ cluster algorithms, we computed the vacuum expectation value

$$v = \langle |\phi| \rangle \quad , \quad \phi \equiv \frac{1}{V_4} \sum_x \phi(x) \quad (39)$$

and the connected propagator

$$G(x) = \langle \phi(x)\phi(0) \rangle - v^2 \quad (40)$$

where $\langle \dots \rangle$ denotes averaging over the lattice configurations.

^jHere, an analogy can help intuition. To this end, one can compare the continuum limit of SSB to the incompressibility limit of a superfluid. In general, this has two types of excitations: low-momentum compressional modes (phonons) and higher momentum vortical modes (rotons). If the sound velocity $c_s \rightarrow \infty$ the phase space of the phonon branch, the analog of the quasi-particles of type I, with energy $E(\mathbf{k}) = c_s|\mathbf{k}|$, would just reduce to the zero-measure set $\mathbf{k} = 0$. Then, in this limit, only rotons, the analog of the quasi-particles of type II, would propagate in the system.

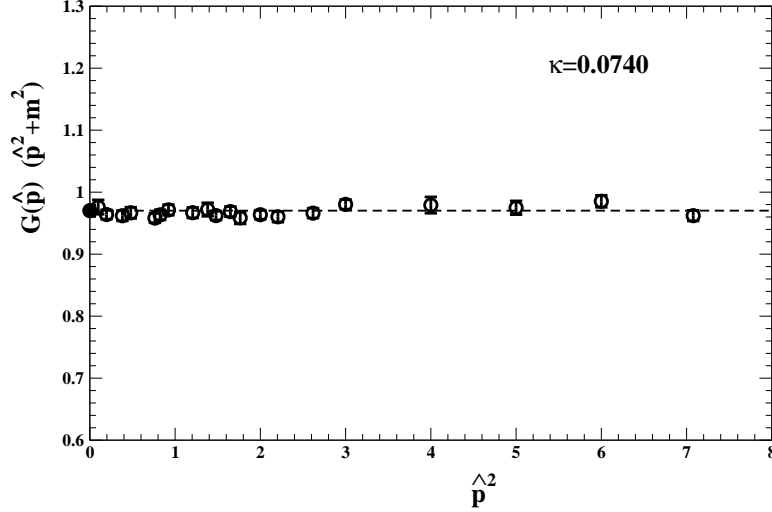


Fig. 2. The lattice data for the re-scaled propagator in the symmetric phase at $\kappa = 0.074$ as a function of the square lattice momentum \hat{p}^2 with $\hat{p}_\mu = 2 \sin p_\mu/2$. The fitted mass is $m_{\text{latt}} = 0.2141(28)$ and the dashed line indicates the value of $Z_{\text{prop}} = 0.9682(23)$. The zero-momentum full point is $Z_\varphi = (2\kappa\chi_{\text{latt}})m_{\text{latt}}^2 = 0.9702(91)$. Data are taken from Ref.²⁸

Our scope was to check the basic relation $M_h^2 \sim m_h^2 \ln(\Lambda_s/M_h)$ where M_h describes the higher momentum propagator and m_h is defined from the zero-momentum 2-point function Eq.(34)

$$m_h^2 \equiv V_{\text{eff}}''(\pm v) = -\Pi(p=0) = |\Pi(p=0)| \quad (41)$$

By introducing the Fourier transform of the propagator $G(p)$, its $p=0$ limit is the susceptibility χ whose conventional definition includes the normalization factor 2κ , i.e. $2\kappa\chi \equiv 2\kappa G(p=0)$. Therefore the extraction of m_h is straightforward

$$2\kappa\chi = 2\kappa G(p=0) = \frac{1}{|\Pi(p=0)|} \equiv \frac{1}{m_h^2} \quad (42)$$

Extraction of M_h requires more efforts. To this end, let us denote by m_{latt} the mass obtained directly from a fit to the propagator data in some region of momentum. If our picture is correct, the difference of the value $M_h \equiv m_{\text{latt}}$, as fitted in the higher-momentum region, from the corresponding $m_h \equiv (2\kappa\chi_{\text{latt}})^{-1/2}$, should become larger and larger in the continuum limit. Namely, the quantity

$$Z_\varphi = \frac{M_h^2}{m_h^2} \equiv m_{\text{latt}}^2 (2\kappa\chi_{\text{latt}}) \quad (43)$$

should exhibit a definite logarithmic increase when approaching the critical point $\kappa \rightarrow \kappa_c$.

This analysis was first performed in Ref.²⁸ for both symmetric and broken phase. The data for the connected propagator $2\kappa G(p)$ were first fitted to the 2-parameter

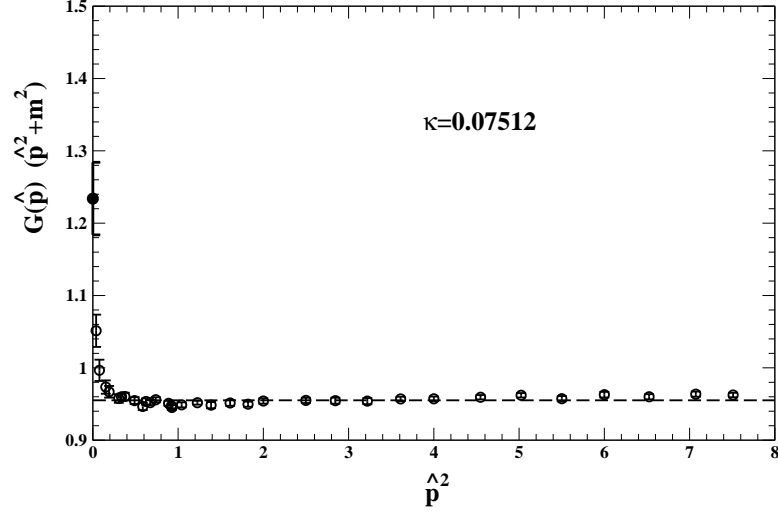


Fig. 3. The lattice data for the re-scaled propagator in the broken phase at $\kappa = 0.07512$ as a function of the square lattice momentum \hat{p}^2 with $\hat{p}_\mu = 2 \sin p_\mu/2$. The fitted mass is $m_{\text{latt}} = 0.2062(41)$ and the dashed line indicates the value of $Z_{\text{prop}} = 0.9551(21)$. The zero-momentum full point is $Z_\varphi = (2\kappa\chi_{\text{latt}})m_{\text{latt}}^2 = 1.234(50)$. Data are taken from Ref.²⁸

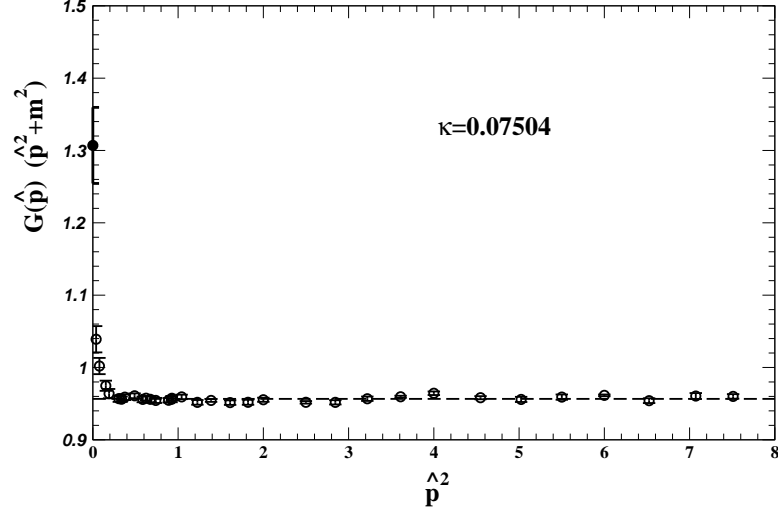


Fig. 4. The lattice data for the re-scaled propagator in the broken phase at $\kappa = 0.07504$ as a function of the square lattice momentum \hat{p}^2 with $\hat{p}_\mu = 2 \sin p_\mu/2$. The fitted mass is $m_{\text{latt}} = 0.1723(34)$ and the dashed line indicates the value of $Z_{\text{prop}} = 0.9566(13)$. The zero-momentum full point is $Z_\varphi = (2\kappa\chi_{\text{latt}})m_{\text{latt}}^2 = 1.307(52)$. Data are taken from Ref.²⁸

form

$$G_{\text{fit}}(p) = \frac{Z_{\text{prop}}}{\hat{p}^2 + m_{\text{latt}}^2} \quad (44)$$

in terms of the squared lattice momentum \hat{p}^2 with $\hat{p}_\mu = 2 \sin p_\mu/2$. The data were then plotted after a re-scaling by the factor $(\hat{p}^2 + m_{\text{latt}}^2)$. In this way, deviations from constancy become clearly visible and indicate how well a given lattice mass can describe the data down to $p \rightarrow 0$.

The results for the symmetric phase, in Fig.2 at $\kappa = 0.074$, show that, there, a single lattice mass works remarkably well in the whole range of momentum down to $p = 0$. Also $Z_\varphi = (2\kappa)m_{\text{latt}}^2\chi_{\text{latt}} = 0.9702(91)$ agrees very well with the fitted $Z_{\text{prop}} = 0.9682(23)$.

In Figs.3 and 4 we then report the analogous plots for the broken-symmetry phase at $\kappa = 0.07512$ and $\kappa = 0.07504$ for $m_{\text{latt}} = 0.2062(41)$ and $m_{\text{latt}} = 0.1723(34)$ respectively. As one can see, the fitted lattice mass describe well the data for not too small values of the momentum but in the $p \rightarrow 0$ limit the deviation from constancy becomes highly significant statistically. To make this completely evident, we show in Fig.5 the normalized chi-square vs. the number of points included in the fit.

Notice that the two quantities $Z_\varphi = (2\kappa)m_{\text{latt}}^2\chi_{\text{latt}} = 1.234(50)$ and $Z_\varphi = (2\kappa)m_{\text{latt}}^2\chi_{\text{latt}} = 1.307(52)$ respectively are now very different from the corresponding quantities $Z_{\text{prop}} = 0.9551(21)$ and $Z_{\text{prop}} = 0.9566(13)$ obtained from the higher-momentum fits. Also, the value of Z_φ increases by approaching the critical point as expected.

The whole issue was thoroughly re-analyzed by Stevenson³⁰ in 2005. For an additional check, he also extracted propagator data from the time-slices for the connected correlator measured by Balog et al.²⁹ for $\kappa = 0.0751$. He found that their higher-momentum data were requiring a mass value $m_{\text{latt}} \sim 0.2$ but, again, see his Fig.6(d), this mass could not describe the very low momentum points, exactly as in our Figs.3 and 4. In connection with the susceptibility $\chi_{\text{latt}} = 206.4(1.2)$ measured by Balog et al. at $\kappa = 0.0751$ (see their Table 3), this gives $Z_\varphi = (2\kappa\chi_{\text{latt}})m_{\text{latt}}^2 \sim 1.24$ in very good agreement with our determination $Z_\varphi = (2\kappa\chi_{\text{latt}})m_{\text{latt}}^2 = 1.234(50)$ at the very close point $\kappa = 0.07512$.

Therefore, data collected by other groups were confirming that in the broken-symmetry phase $M_h \equiv m_{\text{latt}}$, obtained from a fit to the higher-momentum propagator data, and $m_h = (2\kappa\chi_{\text{latt}})^{-1/2}$ become more and more different in the continuum limit.

However since this is still not generally appreciated, and to emphasize the phenomenological implications, we will now display more precisely the predicted logarithmic increase of Z_φ . To this end, we will show that the lattice data give consistent values of the proportionality constant c_2 in Eq.(27)

$$Z_\varphi = \frac{M_h^2}{m_h^2} \equiv (2\kappa\chi_{\text{latt}})m_{\text{latt}}^2 \sim \frac{L}{c_2} \quad (45)$$

where $L \equiv \ln(\Lambda_s/m_{\text{latt}})$. This requires to compute the combination

$$m_{\text{latt}} \sqrt{\frac{2\kappa\chi_{\text{latt}}}{\ln(\pi/am_{\text{latt}})}} \equiv \frac{1}{\sqrt{c_2}} \quad (46)$$

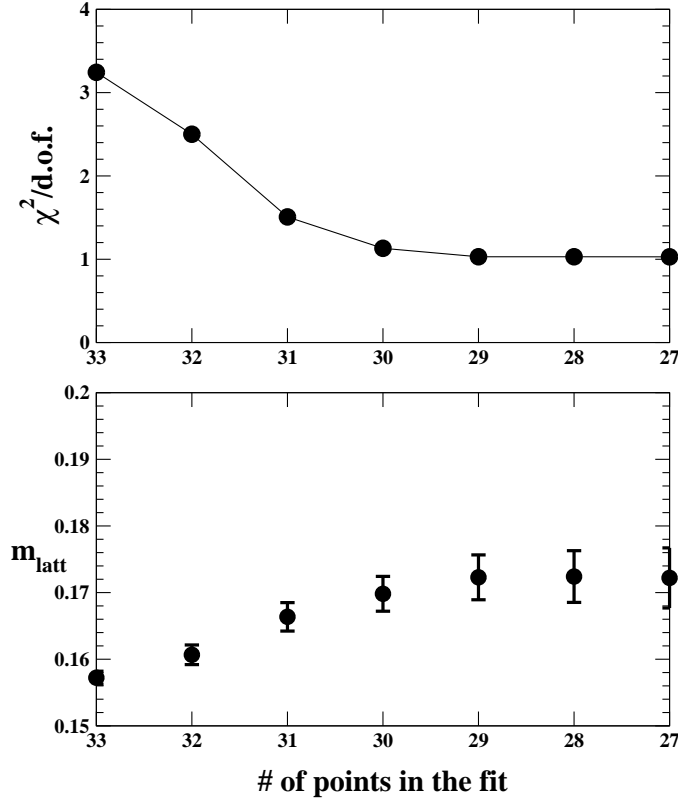


Fig. 5. For $\kappa = 0.07504$ we show the value of the normalized chi-square and the fitted lattice mass depending on the number of points included in the high-energy region. Data are taken from Ref.²⁸

where we have replaced the cutoff $\Lambda_s \sim (\pi/a)$ in terms of the lattice spacing a . In this derivation, no additional theoretical inputs (such as definitions of renormalized mass and coupling constant) are needed. The only two ingredients are i) the direct measurement of the susceptibility and ii) the direct measurements of the connected propagator. The higher-momentum region reproduced by the two-parameter form Eq.(44) is determined by the data themselves and used to extract m_{latt} .

We give first in Table 1 the measured values of the lattice susceptibility at various κ (well within the scaling region). We then report in Table 2 the fitted m_{latt} together with the other quantities entering the determination of the coefficient c_2 in Eq.(46). The spread of the central values at $\kappa = 0.0749$ reflects the theoretical uncertainty in the choice of the higher-momentum range, $\hat{p}^2 > 0.1$ and $\hat{p}^2 > 0.2$ respectively. Only the region $\hat{p}^2 < 0.1$ cannot be consistently considered with the rest of the data, see Fig.6. In this low-momentum range the propagator data would

Table 1. The values of the susceptibility at various κ . The results for $\kappa = 0.07512$ and $\kappa = 0.07504$ are taken from ref.²⁸ The result for $\kappa = 0.0751$ is taken from ref.²⁹ while the other value at $\kappa = 0.0749$ derives from our new simulations on a 76^4 lattice.

κ	lattice	χ_{latt}
0.07512	32^4	193.1(1.7)
0.0751	48^4	206.4(1.2)
0.07504	32^4	293.38(2.86)
0.0749	76^4	1129(24)

Table 2. The values of m_{latt} , as obtained from a direct fit to the higher-momentum propagator data, are reported together with the other quantities entering the determination of the coefficient c_2 in Eq.(46). The entries at $\kappa = 0.07512$ and $\kappa = 0.07504$ are taken from ref.²⁸ The susceptibility at $\kappa = 0.0751$ is directly reported in ref.²⁹ The corresponding mass at $\kappa = 0.0751$ was extracted by Stevenson³⁰ (see his Fig.6(d)) by fitting to the higher-momentum data of ref.²⁹ The two entries at $\kappa = 0.0749$, from our new simulations on a 76^4 lattice, refer to higher-momentum fits for $\hat{p}^2 > 0.1$ and $\hat{p}^2 > 0.2$ respectively.

κ	m_{latt}	$(2\kappa\chi_{\text{latt}})^{1/2}$	$[\ln(\Lambda_s/m_{\text{latt}})]^{-1/2}$	$(c_2)^{-1/2}$
0.07512	0.2062(41)	5.386(23)	0.606(2)	0.673(14)
0.0751	~ 0.200	5.568(16)	~ 0.603	~ 0.671
0.07504	0.1723(34)	6.636(32)	0.587(2)	0.671(14)
0.0749	0.0933(28)	13.00(14)	0.533(2)	0.647(20)
0.0749	0.100(6)	13.00(14)	0.538(4)	0.699(42)

in fact require the same mass parameter $m_h = (2\kappa\chi_{\text{latt}})^{-1/2} = 0.0769$ fixed by the inverse susceptibility, see Fig.7.

The reason of this uncertainty is that, differently from the simulations at $\kappa = 0.07512$ and $\kappa = 0.07504$, this higher-momentum range cannot be uniquely determined by simply imposing a normalized chi-square of order unity as in Fig.5. To this end, in fact, statistical errors should be reduced by, at least, a factor of 2 with a corresponding increase of the CPU time by a factor 4. Due to the large size 76^4 of the lattice needed to run a simulation at $\kappa = 0.0749$, this increase in statistics would take several additional months.

Nevertheless, with our present statistics this type of uncertainty can be translated into the average estimate $m_{\text{latt}} \sim 0.096(3)$ at $\kappa = 0.0749$, or $1/\sqrt{c_2} \sim 0.67 \pm 0.02$. In turn, besides the statistical errors, this is equivalent to a systematic error ± 0.02 in the final average

$$\frac{1}{\sqrt{c_2}} = 0.67 \pm 0.01(\text{stat}) \pm 0.02(\text{sys}) \quad (47)$$

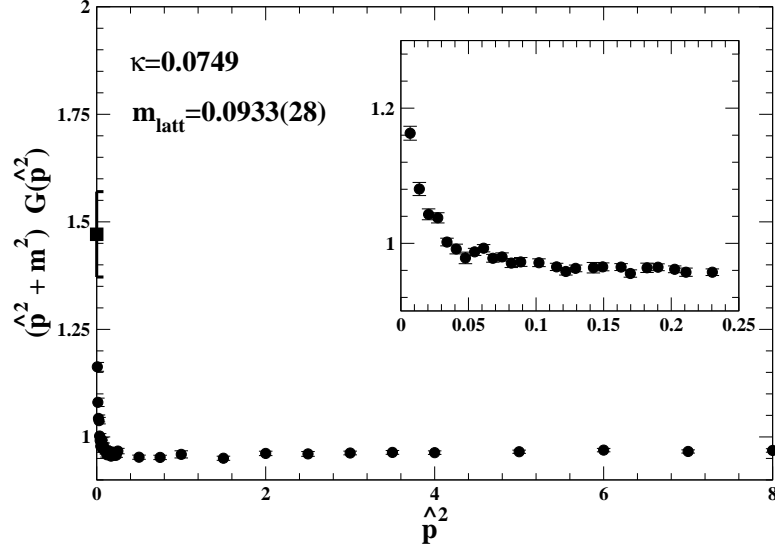


Fig. 6. The propagator data, at $\kappa = 0.0749$, rescaled with the lattice mass $m_{\text{latt}} = 0.0933(28)$ obtained from the fit to all data with $\hat{p}^2 > 0.1$. The square at $p = 0$ is $Z_\varphi = m_{\text{latt}}^2 (2\kappa\chi_{\text{latt}}) = 1.47(9)$.

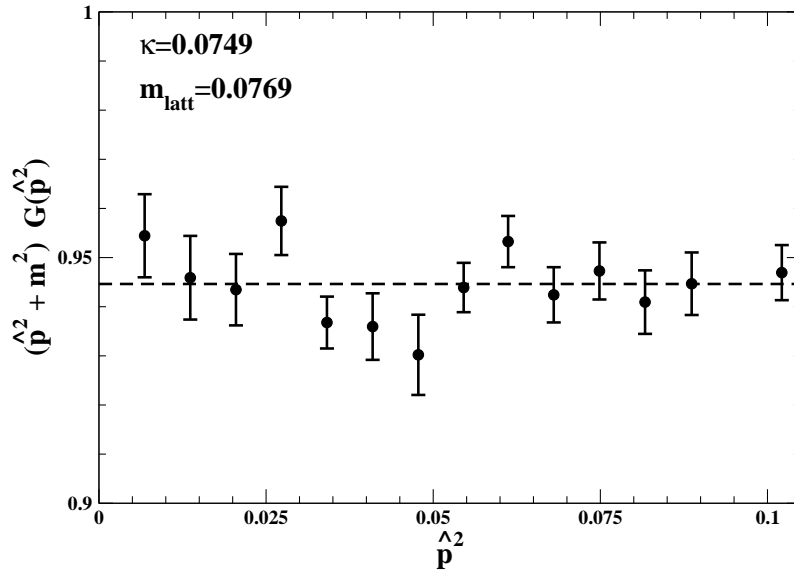


Fig. 7. The propagator data at $\kappa = 0.0749$ for $\hat{p}^2 < 0.1$. The lattice mass used here for the rescaling was fixed at the value $m_h \equiv (2\kappa\chi_{\text{latt}})^{-1/2} = 0.0769$.

With this determination, we can then compare with the Lüscher-Weisz scheme³¹

20 *M. Consoli, L. Cosmai*

where mass m_R , coupling constant^k λ_R and weak scale $\langle\Phi\rangle$ are related through the relation

$$\frac{m_R^2}{\langle\Phi\rangle^2} = \frac{\lambda_R}{3} \quad (48)$$

and the mass is expressed in terms of the zero-momentum propagator as

$$\frac{Z_R}{m_R^2} = G(p=0) = 2\kappa\chi = \frac{1}{m_h^2} \quad (49)$$

through a perturbative rescaling $Z_R \lesssim 1$.

Traditionally, Eq.(48) has been used to place upper bounds on the Higgs boson mass depending on the value of $\lambda_R \sim (1/L)$ and thus on the magnitude of Λ_s . Instead, in our case, where $M_h^2 \sim Lm_h^2 \sim Lm_R^2$, it can be used to express the value of M_h in units of $\langle\Phi\rangle$ because the two quantities now scale uniformly, see Eq.(29). Since our estimate of the $M_h - m_h$ relation just takes into account the leading-order logarithmic effect, in a first approach, we will neglect the non-leading quantity Z_R and, as sketched at the end of Sect.2, approximate $m_R \sim m_h$. Therefore, by using the leading-order relation $(m_h/\langle\Phi\rangle)^2 \sim 16\pi^2/(9L)$, Eq.(45) and the average value Eq.(47), the logarithmic divergent L drops out and we find

$$\frac{M_h}{\langle\Phi\rangle} = \sqrt{\frac{m_h^2}{\langle\Phi\rangle^2} \frac{M_h^2}{m_h^2}} \sim \sqrt{\frac{16\pi^2}{9L} \frac{L}{c_2}} = 2.81 \pm 0.04(\text{stat}) \pm 0.08(\text{sys}) \quad (50)$$

or, for $\langle\Phi\rangle \sim 246$ GeV,

$$M_h = 690 \pm 10(\text{stat}) \pm 20(\text{sys}) \text{ GeV} \quad (51)$$

We observe that the above value is slightly smaller but consistent with our previous estimate^{32,33}

$$M_h = 754 \pm 20(\text{stat}) \pm 20(\text{sys}) \text{ GeV} \quad (52)$$

This had been obtained, within the same Lüscher-Weisz scheme, but using instead the full chain

$$\frac{M_h}{\langle\Phi\rangle} = \sqrt{\frac{M_h^2}{m_h^2} \frac{m_h^2}{m_R^2} \frac{m_R^2}{\langle\Phi\rangle^2}} = \sqrt{\frac{Z_\varphi}{Z_R} \frac{\lambda_R}{3}} \quad (53)$$

and thus account for both the logarithmic divergent Z_φ and the non-leading correction Z_R .

This old estimate Eq.(52) can now be compared with our new determination of Z_φ from the direct measurement of the lattice propagator. To eliminate any explicit dependence on the lattice mass it is convenient to introduce the traditional divergent log used to describe the continuum limit of the Ising model³⁴

$$L(k) = \frac{1}{2} \ln \frac{\kappa_c}{\kappa - \kappa_c} \quad (54)$$

^kIn the Lüscher-Weisz paper the scalar self coupling is called g . However, here, to avoid possible confusion with the gauge couplings we will maintain the traditional notation λ .

and define a set of values

$$Z_\varphi \equiv \frac{L(k)}{c_2} \quad (55)$$

at the various κ . By using our Eq.(47) and $\kappa_c = 0.0748474(3)$, all entries needed in Eq.(53) are reported in Table 3. Then, by averaging at the various κ , the new determination $M_h \sim 752 \pm 20$ GeV is the same value Eq.(52) obtained in refs.^{32,33}

Table 3. We report the original Lüscher-Weisz entries³¹ λ_R and Z_R , the rescaling $\sqrt{Z_\varphi} \equiv \sqrt{\frac{L(k)}{c_2}}$, with $L(k)$ as in Eq.(54) and $1/\sqrt{c_2} = 0.670 \pm 0.023$ as in Eq.(47), together with the resulting M_h from Eq.(53).

κ	λ_R	Z_R	$\sqrt{Z_\varphi}$	M_h (GeV)
0.0759	27(2)	0.929(14)	0.98(3)	751 (37)
0.0754	24(2)	0.932(14)	1.05(4)	757 (40)
0.0751	20(1)	0.938(12)	1.13(4)	742 (33)
0.0749	16.4(9)	0.944(11)	1.28(5)	758 (34)

One may object that the new precise κ_c is marginally consistent with the old value 0.07475(7) used originally by Lüscher-Weisz³¹ to compute the λ_R 's and Z_R 's reported in Table 3. However, Z_R is a very slowly varying, non-leading quantity whose dependence on the critical point is well within the uncertainties reported in Table 3. Also, the dependence of λ_R on the various mass scales is only logarithmic and possible differences are further flattened because only $\sqrt{\lambda_R}$ enters the determination of M_h ¹.

We thus conclude that, either with the original estimate of refs.^{32,33} or with our new determination of Z_φ in Table 3, Eq.(53) remains as an alternative approach to M_h which has its own motivations and takes also into account the average +3% effect embodied in $\sqrt{Z_R} \sim 0.97$. In this perspective, Eqs.(51) and (52) could be combined in a final estimate

$$M_h = 720 \pm 30 \text{ GeV} \quad (56)$$

which incorporates the various statistical and theoretical uncertainties.

6. Summary and outlook

In the first version of the theory, with a classical scalar potential, the sector inducing SSB was quite distinct from the remaining self-interactions of the Higgs field induced through its gauge and Yukawa couplings. In this paper, we have adopted a similar

¹With a critical $\kappa_c = 0.074848$ very close to the present most precise determination $\kappa_c = 0.0748474(3)$, the λ_R 's were re-computed by Stevenson,³⁰ see his Fig.1 (f). His new central values are about $\lambda_R = 30, 25, 21, 16.7$ for $\kappa = 0.0759, 0.0754, 0.0751$ and 0.0749 respectively and thus within the uncertainties reported in Table 3. In any case, the average +2.7% increase in the central value of M_h remains within the ± 20 GeV systematic error reported in Eq.(52).

perspective but, following most recent lattice simulations, described SSB in $\lambda\Phi^4$ theory as a weak first-order phase transition.

In the approximation schemes we have considered, there are two different mass scales. On the one hand, a mass m_h defined by the quadratic shape of the effective potential at its minimum and related to the zero-momentum self-energy $\Pi(p=0)$. On the other hand, a second mass M_h , defined by the zero-point energy which is relevant for vacuum stability and related to a typical average value $\langle\Pi(p)\rangle$ at larger $|p|$.

So far, these two scales have always been considered as a single mass but our results indicate instead the order of magnitude relation $M_h^2 \sim m_h^2 L \gg m_h^2$, where $L = \ln(\Lambda_s/M_h)$ and Λ_s is the ultraviolet cutoff of the scalar sector which induces SSB. We have checked this two-scale structure with lattice simulations of the propagator and of the susceptibility in the 4D Ising limit of the theory. These confirm that, by approaching the critical point, M_h^2 , as extracted from a fit to the higher-momentum propagator data, increases logarithmically in units of m_h^2 , as defined from the inverse zero-momentum susceptibility $|\Pi(p=0)| = (2\kappa\chi)^{-1}$. At the same time, see Fig.7, $m_h = (2\kappa\chi)^{-1/2}$ is the right mass to describe the propagator in the low-momentum region. Therefore, in a cutoff theory where both m_h and M_h are finite, one should think of the scalar propagator as a smooth interpolation between these two masses.

With the aim of extending our description of SSB to more ambitious frameworks, we have also developed in Sect.2 a RG-analysis which, in principle, could also be extended to the $\Lambda_s \rightarrow \infty$ limit and introduces two invariants \mathcal{I}_1 and \mathcal{I}_2 . The former is related to the vacuum energy $\mathcal{E} \sim -M_h^4$, through the relation $\mathcal{I}_1 = M_h$. The latter is the natural candidate to represent the weak scale $\langle\Phi\rangle \sim 246$ GeV through the relation $\mathcal{I}_2 = \langle\Phi\rangle$.

Therefore since, differently from m_h , the larger mass M_h remains finite in units of $\langle\Phi\rangle$ in the continuum limit, one can write a proportionality relation, say $M_h = K\langle\Phi\rangle$, and extract the constant K from lattice simulations. As discussed in Sect.5, this leads to our final estimate $M_h \sim 720 \pm 30$ GeV which incorporates various statistical and theoretical uncertainties.

The existence of two masses in our picture of SSB leads to exploit the natural identification of our lower mass m_h with the present experimental value 125 GeV. In this case, we obtain

$$\frac{M_h}{125 \text{ GeV}} \sim \sqrt{\frac{L}{c_2}} \quad (57)$$

so that from

$$M_h \sim \frac{4\pi\langle\Phi\rangle}{3\sqrt{c_2}} \quad (58)$$

we find $\sqrt{L} \sim 8.25$. When taken at face value, this would imply a scalar cutoff $\Lambda_s \sim 2.6 \cdot 10^{32}$ GeV which is much larger than the Planck scale. But, as pointed out

in the footnote before Eq.(19), this may be just a cutoff artifact because to obtain the same physical M_h from Eq.(10) and Eq.(19) one should use vastly different values of the ultraviolet cutoff.

Instead, as emphasized in the Introduction, our aim was to give a cutoff-independent description of symmetry breaking in $\lambda\Phi^4$ theory, i.e. a description that could also remain valid in the $\Lambda_s \rightarrow \infty$ limit. In this perspective, for an experimental check of our picture, we should first look at the *cutoff-independent* $M_h - \langle\Phi\rangle$ relation. Since this would imply the existence of a new scalar resonance around 700 GeV, we will now briefly recall some experimental signals from LHC that may support this prediction. The $M_h - m_h$ relative magnitude will be re-discussed afterwards by making use of a physical, measurable quantity.

Let us start with the 2-photon channel. At the time of 2016, both ATLAS³⁵ and CMS³⁶ experiments reported an excess of events in the 2-photon channel that could indicate a new narrow resonance around 750 GeV. The collisions were recorded at center of mass energy of 8 and 13 TeV and the local statistical significance of the signal was estimated to be 3.8 sigma by ATLAS and 3.4 sigma by CMS. Later on, with more statistics, the two Collaborations reported a considerable reduction in the observed effect. For ATLAS³⁷ the local deviation from the background-only hypothesis was reduced to 1.8 sigma while for CMS,³⁸ the original 3.4 sigma effect was now lowered to about 1.9 sigma. Yet, in spite of the reported modest statistical significance, if one looks at the 2-photon invariant mass distribution in figure 2a of ATLAS,³⁷ an excess of events at about 730 GeV is clearly visible. Interestingly, this excess is immediately followed by a strong decrease in the number of events. This may indicate the characteristic $(M^2 - s)$ effect due to the (negative) interference of a resonance of mass M with a non-resonating background. These last papers were published in 2017 and the total integrated luminosity was 36 fb^{-1} ($12.9 + 19.7 + 3.3$) for CMS and 36.7 fb^{-1} for ATLAS. This is just a small fraction of the full present statistics of about 140 fb^{-1} per experiment.

Let us now consider the “golden” 4-lepton channel at large values of the invariant mass $m_{4l} > 600 \text{ GeV}$. For the latest paper by ATLAS,³⁹ with a statistics of 36.1 fb^{-1} , one can look at their figure 4a. Again, as in their corresponding 2-photon channel (the mentioned figure 2a of³⁷), there is a clean excess of events for $m_{4l} = 700 \text{ GeV}$ where the signal exceeds the background by about a factor of three. At the closest points, 680 and 720 GeV, the signal becomes consistent with the background within 1 sigma but the central values are still larger than the background by a factor of two. The other paper by CMS⁴⁰ refers to a statistics of 77.4 fb^{-1} but the results in the region $m_{4l} \sim 700 \text{ GeV}$, illustrated in their Fig.9, cannot be easily interpreted.

However, here, an independent analysis of these data by Cea¹¹ can greatly help. The extraction of the CMS data and their combination with the ATLAS data presented in Figures 1 and 2 of ref.¹¹ indicates an evident excess in the 4-lepton final state with a statistical significance of about 5 sigma. The natural interpretation of this excess would be in terms of a scalar resonance, with a mass of about 700

GeV, which decays into two Z bosons and then into leptons. We emphasize that one does not need to agree with Cea's theoretical model to appreciate his analysis of the data. Therefore, if this excess will be confirmed, it could represent the second heavier mass scale discussed in our paper. We emphasize that the statistical sample used in¹¹ is the whole official set of data available at present, namely 113.5 fb^{-1} (36.1 for ATLAS + 77.4 for CMS). Again, as for the 2-photon case, this is still far from the nominal collected luminosity of about 140 fb^{-1} per experiment.

In this situation, where only a small fraction of the full statistics has been made available, further speculations on the characteristics of a hypothetical heavy mass state at 700 GeV may be premature. Nevertheless, even though this scale is not far from the usual triviality bounds, the actual situation we expect is very different. In fact these bounds have been obtained for $M_h \lesssim \Lambda_s$ while we are now considering a corner of the parameter space, i.e. large M_h with $M_h \ll \Lambda_s$, that does not exist in the conventional treatment. For this reason the phenomenology of such heavy resonance (i.e. its production cross sections and decay rates) may differ sizeably from the perturbative expectations. In particular, differently from the low-mass state at 125 GeV, the decay width of the heavy state into longitudinal vector bosons will be crucial to determine the strength of the scalar self-interaction. We thus return to the previous issue concerning the relative magnitude of M_h and m_h .

From the experimental ATLAS + CMS papers that we have considered, the total width of this hypothetical heavy resonance can hardly exceed 40 GeV. For a mass of 720 GeV, about 30 GeV of this width, those into heavy and light fermions, gluons, photons...would certainly be there. Thus, the decay width into W's and Z's should be of the order of 10 GeV, or less. The observation of such a heavy but narrow resonance would then confirm the scenario of ref.⁴¹ where, with a heavy Higgs particle, re-scattering of longitudinal vector bosons was effectively reducing their large tree-level coupling and thus the decay width in that channel. In the language of the present paper, this could be expressed by saying that the tree-level estimate $\Gamma_0(h \rightarrow V_L V_L) \sim M_h^3 G_{\text{Fermi}} \sim 175 \text{ GeV}$ becomes the much smaller value $\Gamma(h \rightarrow V_L V_L) \sim M_h(m_h^2 G_{\text{Fermi}})$ where M_h is from phase space and $m_h^2 G_F$ is the reduced strength of the interaction. If M_h is close to 720 GeV and the mass m_h needed for the reduction of the width is close to 125 GeV, say a width into vector bosons of the order of 5 GeV, this would then close the circle and lead to the identification $m_h \sim 125 \text{ GeV}$.

Finally, the simultaneous presence of two different mass scales in the Higgs field propagator would also require some interpolating form, of the type Eq.(37), in the loop corrections. Since some precision measurements (e.g. the b-quark forward-backward asymmetry or the value of $\sin^2 \theta_w$ from neutral current experiments^m) still point to a rather large Higgs particle mass, with about 3-sigma discrepancies, this could provide an alternative way to improve the overall quality of a Standard Model fit.

^mFor a general discussion of the various quantities and of systematic errors see ref.⁴²

References

1. P. W. Higgs, *Phys. Lett.* **12**, 132 (1964), doi:10.1016/0031-9163(64)91136-9.
2. F. Englert and R. Brout, *Phys. Rev. Lett.* **13**, 321 (1964), doi:10.1103/PhysRevLett.13.321.
3. ATLAS Collaboration (G. Aad *et al.*), *Phys. Lett.* **B716**, 1 (2012), [arXiv:1207.7214 \[hep-ex\]](#), doi:10.1016/j.physletb.2012.08.020.
4. CMS Collaboration (S. Chatrchyan *et al.*), *Phys. Lett.* **B716**, 30 (2012), [arXiv:1207.7235 \[hep-ex\]](#), doi:10.1016/j.physletb.2012.08.021.
5. S. R. Coleman and E. J. Weinberg, *Phys. Rev.* **D7**, 1888 (1973), doi:10.1103/PhysRevD.7.1888.
6. P. H. Lundow and K. Markström, *Physical Review E* **80**, 031104 (2009).
7. P. H. Lundow and K. Markstrom, *Nucl. Phys.* **B845**, 120 (2011), [arXiv:1010.5958 \[cond-mat.stat-mech\]](#), doi:10.1016/j.nuclphysb.2010.12.002.
8. S. Akiyama, Y. Kuramashi, T. Yamashita and Y. Yoshimura, *Physical Review D* **100**, 054510 (2019).
9. M. Consoli and P. M. Stevenson, *Int. J. Mod. Phys.* **A15**, 133 (2000), [arXiv:hep-ph/9905427 \[hep-ph\]](#), doi:10.1142/S0217751X00000070.
10. Particle Data Group Collaboration (M. Tanabashi *et al.*), *Phys. Rev. D* **98**, 030001 (2018), doi:10.1103/PhysRevD.98.030001.
11. P. Cea, *Mod. Phys. Lett.* **A34**, 1950137 (2019), [arXiv:1806.04529 \[hep-ph\]](#), doi:10.1142/S0217732319501372.
12. L. Dolan and R. Jackiw, *Phys. Rev.* **D9**, 2904 (1974), doi:10.1103/PhysRevD.9.2904.
13. M. Consoli and P. M. Stevenson, *Z. Phys.* **C63**, 427 (1994), [arXiv:hep-ph/9310338 \[hep-ph\]](#), doi:10.1007/BF01580323.
14. M. Consoli and P. M. Stevenson, *Phys. Lett.* **B391**, 144 (1997), doi:10.1016/S0370-2693(96)01436-0.
15. T. Barnes and G. I. Ghandour, *Phys. Rev.* **D22**, 924 (1980), doi:10.1103/PhysRevD.22.924.
16. P. M. Stevenson, *Phys. Rev.* **D32**, 1389 (1985), doi:10.1103/PhysRevD.32.1389.
17. H. W. L. Naus, T. Gasenzer and H. J. Pirner, *Annalen Phys.* **6**, 287 (1997), [arXiv:hep-ph/9507357 \[hep-ph\]](#), doi:10.1002/andp.19975090403.
18. A. Okopinska, *Phys. Lett.* **B375**, 213 (1996), [arXiv:hep-th/9508087 \[hep-th\]](#), doi:10.1016/0370-2693(96)00198-0.
19. I. Stancu and P. M. Stevenson, *Phys. Rev.* **D42**, 2710 (1990), doi:10.1103/PhysRevD.42.2710.
20. P. Cea and L. Tedesco, *Phys. Rev.* **D55**, 4967 (1997), [arXiv:hep-th/9607156 \[hep-th\]](#), doi:10.1103/PhysRevD.55.4967.
21. P. M. Stevenson, *Mod. Phys. Lett.* **A24**, 261 (2009), [arXiv:0806.3690 \[hep-ph\]](#), doi:10.1142/S0217732309028990.
22. G. Feinberg and J. Sucher, *Phys. Rev.* **166**, 1638 (1968), doi:10.1103/PhysRev.166.1638.
23. G. Feinberg, J. Sucher and C. K. Au, *Phys. Rept.* **180**, 83 (1989), doi:10.1016/0370-1573(89)90111-7.
24. C. B. Lang, *NATO Sci. Ser. C* **449**, 133 (1994), [arXiv:hep-lat/9312004 \[hep-lat\]](#).
25. I. Montvay and G. Münster, *Quantum fields on a lattice* (Cambridge University Press, 1997).
26. R. H. Swendsen and J.-S. Wang, *Phys. Rev. Lett.* **58**, 86 (1987), doi:10.1103/PhysRevLett.58.86.
27. U. Wolff, *Phys. Rev. Lett.* **62**, 361 (1989), doi:10.1103/PhysRevLett.62.361.
28. P. Cea, M. Consoli, L. Cosmai and P. M. Stevenson, *Mod. Phys. Lett.* **A14**, 1673

26 *M. Consoli, L. Cosmai*

- (1999), [arXiv:hep-lat/9902020](#) [hep-lat], doi:10.1142/S0217732399001760.
29. J. Balog, A. Duncan, R. Willey, F. Niedermayer and P. Weisz, *Nucl. Phys.* **B714**, 256 (2005), [arXiv:hep-lat/0412015](#) [hep-lat], doi:10.1016/j.nuclphysb.2005.01.005.
 30. P. M. Stevenson, *Nucl. Phys.* **B729**, 542 (2005), [arXiv:hep-lat/0507038](#) [hep-lat], doi:10.1016/j.nuclphysb.2005.09.015.
 31. M. Luscher and P. Weisz, *Nucl. Phys.* **B295**, 65 (1988), doi:10.1016/0550-3213(88)90228-3.
 32. P. Cea, M. Consoli and L. Cosmai, *Nucl. Phys. Proc. Suppl.* **129**, 780 (2004), [arXiv:hep-lat/0309050](#) [hep-lat], doi:10.1016/S0920-5632(03)02711-7, [780(2003)].
 33. P. Cea and L. Cosmai, *ISRN High Energy Phys.* **2012**, 637950 (2012), [arXiv:0911.5220](#) [hep-ph], doi:10.5402/2012/637950.
 34. J. Zinn-Justin, *Int. Ser. Monogr. Phys.* **113**, 1 (2002).
 35. ATLAS Collaboration (M. Aaboud *et al.*), *JHEP* **09**, 001 (2016), [arXiv:1606.03833](#) [hep-ex], doi:10.1007/JHEP09(2016)001.
 36. CMS Collaboration (V. Khachatryan *et al.*), *Phys. Rev. Lett.* **117**, 051802 (2016), [arXiv:1606.04093](#) [hep-ex], doi:10.1103/PhysRevLett.117.051802.
 37. ATLAS Collaboration (M. Aaboud *et al.*), *Phys. Lett.* **B775**, 105 (2017), [arXiv:1707.04147](#) [hep-ex], doi:10.1016/j.physletb.2017.10.039.
 38. CMS Collaboration (V. Khachatryan *et al.*), *Phys. Lett.* **B767**, 147 (2017), [arXiv:1609.02507](#) [hep-ex], doi:10.1016/j.physletb.2017.01.027.
 39. ATLAS Collaboration (M. Aaboud *et al.*), *Eur. Phys. J.* **C78**, 293 (2018), [arXiv:1712.06386](#) [hep-ex], doi:10.1140/epjc/s10052-018-5686-3.
 40. CMS Collaboration, Measurements of properties of the Higgs boson in the four-lepton final state at $s = 13$ TeV, CMS PAS HIG-18-001(2018).
 41. P. Castorina, M. Consoli and D. Zappala', *J. Phys.* **G35**, 075010 (2008), [arXiv:0710.0458](#) [hep-ph], doi:10.1088/0954-3899/35/7/075010.
 42. M. S. Chanowitz, *Phys. Atom. Nucl.* **73**, 680 (2010), [arXiv:0903.2497](#) [hep-ph], doi:10.1134/S1063778810040149.